Fast Fault Protection Based on Direction of Fault Current for the High-Surety Power-Supply System

Haijin Li, Min Chen, *Member, IEEE*, Boping Yang, Frede Blaabjerg, *Fellow, IEEE*, and Dehong Xu, *Fellow, IEEE*

***Abstract*—The high-surety power-supply system, super uninterruptable power supply (Super-UPS), is an evolution of the traditional uninterruptible power supply. It consists of multiple sources, multiple energy storages, and redundant power converters to improve the reliability of the power-supply system significantly. In this paper, a fast fault-protection scheme based on direction of fault current without the assistance of communication for Super-UPS is presented. It achieves fast and selective fault detection and ensures the uninterruptible load power when short-circuit faults occur. The directional fault-current detection and the coordination between the circuit breakers and converters are investigated. The protection threshold settings are also discussed. In addition, an improved fault-current measurement method, which can suppress the influence of stray inductance of the solid-state circuit breaker, is presented to guarantee an accurate operation of the protection scheme for rapidly rising fault current. Finally, the proposed protection scheme and the improved fault-current measurement method for Super-UPS are verified by experiments.**

***Index Terms*—Directional protection, high-surety power supply, short-circuit fault protection, solid-state circuit breaker (SSCB), uninterruptable power supply (UPS).**

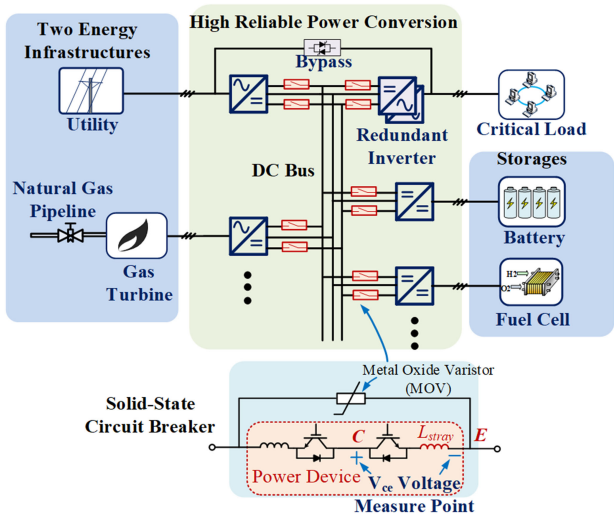

I. Introduction

UNINTERRUPTABLE power supplies (UPSs) have been widely used in Internet data centers (IDCs), telecommunications, factories, etc. Continuous and high-quality power is needed to guarantee the operation of critical loads during power faults due to power aging, extreme weather, or disasters. With the increasing amount of UPS capacity, the requirement of reliability also increases since the higher losses will be caused by the blackout. The concept of the high-surety power supply, namely Super-UPS, is proposed in [1]. It is an evolution of the traditional UPS. The architecture of a Super-UPS is shown in Fig. 1. It consists of multiple sources, multiple energy storages, and redundant power converters to improve the reliability of

Manuscript received February 2, 2018; revised April 29, 2018 and July 27, 2018; accepted September 4, 2018. Date of publication September 17, 2018; date of current version April 20, 2019. This work was supported by the National Natural Science Foundation of China under Grant 51337009. Recommended for publication by Associate Editor Z. Li. *(Corresponding authors: Min Chen and Dehong Xu.)*

H. Li, M. Chen, B. Yang, and D. Xu are with the College of Electrical Engineering, Zhejiang University, Hangzhou, 310027, China (e-mail:

TABLE I
COMPARISON OF DIFFERENT PROTECTION SCHEMES

Method	Merit	Shortcoming
Overcurrent Protection	Fast, reliable	Low selectivity
Current Derivative Protection	Fast, low current threshold	Sensitive to noises and system parameters
Distance protection	Not affected by operation conditions and short-circuit capacity	Sensitive to transient current and noises
Directional Overcurrent Protection	Selectivity for bi-directional power flow systems	Only suitable for radial systems
Directional Comparison Protection	High selectivity	Depends on the low bandwidth communication
Differential Protection	High selectivity, detects high impedance faults	Depends on the high bandwidth communication

of dc systems are investigated by previous works [8]–[28]. The conventional dc protection schemes and the brief comparison of different schemes are shown in Table I [8]–[29], [33]–[36]. The differential protection and directional comparison protection are communication-based protections [17], [23], [26], [27], [36]. They are highly accurate schemes with an optimized selectivity. However, they highly depend on the communication. For the compact and highly reliable power supply, Super-UPS, communication-based protections are not suitable because of relatively slow protection speed. The distance protection, overcurrent protection, derivative protection, and directional overcurrent protection are the noncommunication based protection. The distance protection is not affected by operation conditions and short-circuit capacity [10], [22]. However, it is easily affected by the transient current and noises. It usually requires intense computing capabilities. For Super-UPS, due to the low line impedance of the power supply, the distance protection has low discriminability for the fault location. The overcurrent protection [19] and current derivative protection [20], [21], [24] can provide a fast fault detection, but they cannot achieve selectivity in the multiple-source system with bidirectional power flow such as Super-UPS. The directional overcurrent protection [35] is proposed to locate the feeder fault in the radial system with multiple sources. For Super-UPS, the directional overcurrent protection cannot achieve selectivity protection for all types of faults. In addition, the noncommunication protection and communication-based protection are combined in [17], [33], and [34]. In the combination scheme, the overcurrent protection is used to isolate the load or source fault quickly. The communication-based protection is applied to isolate bus faults. The protection speed is thereby improved. However, due to partially relying on the communication, it may cause temporary load interruptions in compact systems with fast increasing fault current. Thus, the existing methods cannot achieve uninterruptible load power with fast protection in Super-UPS. A fast and reliable, noncommunication based, protection scheme is required for the Super-UPS.

In addition, for the protection methods based on the current detection, the measurement of rapidly rising high fault current is a big challenge in the compact system. Current-measurement methods consist of current transformers (CTs), Rogowski coils, Hall-effect sensors, shunt resistors, and the methods based on the voltage drop of power devices [3]–[7], [23], [30]. The main challenge for CTs and Rogowski coils is that dc component of current cannot be measured. The drawback of current shunt resistors is additional power losses [23]. The disadvantage of Hall-effect sensors is the high cost. If SSCBs are applied in the protection [3]–[7], the voltage drop of the power devices can be used to measure the fault current due to the low cost. However, the voltage drop of power device is affected by temperature. A temperature compensation method has been introduced in [7] and [32]. Besides, the stray inductor of SSCBs, shown in Fig. 1, causes extra voltage drop on the measurement of V_{ce}. The measurement error is large when the derivative of the current is high. In order to achieve an accurate protection, the extra voltage drop caused by the stray inductor of SSCB should be extracted and compensated. The current-measurement method with compensation of the influence of stray inductance is studied in this paper.

In this paper, a fast and reliable protection scheme is proposed for Super-UPS, which is a compact and high-surety power supply. The scheme achieves fast fault detection based on direction of current and coordinates with converters to ensure the uninterruptible load power. It does not rely on any communication. The protection speed and system reliability are improved. Then, an improved fault-current measurement method is presented. The method eliminates the influence of stray inductance of SSCB on the measurement of the rapidly rising fault current. The accuracy of the protection scheme is also improved.

The rest of the paper is organized as follows. In Section II, a fault model is built, and the characteristic of fault-current direction is analyzed. In Section III, a fast protection scheme based on the direction of fault current is developed. In addition, an improved measurement method for rapidly rising fault current is introduced. In Section IV, the prototype of Super-UPS is built, and experimental results are provided. Finally in Section V, the conclusions are given.

II. FAULT MODEL AND ANALYSIS OF SUPER-UPS

A. Fault Types of Super-UPS

The architecture of Super-UPS can be considered as a single-bus radial system. The protection zones in Super-UPS can be divided into module protection zones and the busbar protection zone, which are shown in Fig. 2. In this section, the module fault is analyzed in detail.

The dc bus of a Super-UPS has three poles including a positive pole, a neutral pole, and a negative pole. There are four short-circuit fault types of the module fault. They are positive pole short circuited with negative pole, positive pole short circuited with neutral pole, negative pole short circuited with neutral pole, and all three poles short circuited together.

B. Simplified Fault Model

The circuit model of a Super-UPS is shown in Fig. 3(a). The topologies with neutral point of dc bus are chosen due to the requirement of UPS. In UPS systems, the load inverter is required

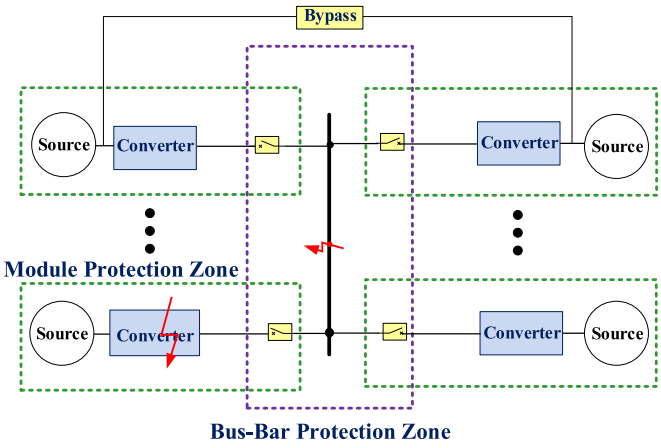

Fig. 2. Protection zones in Super-UPS.

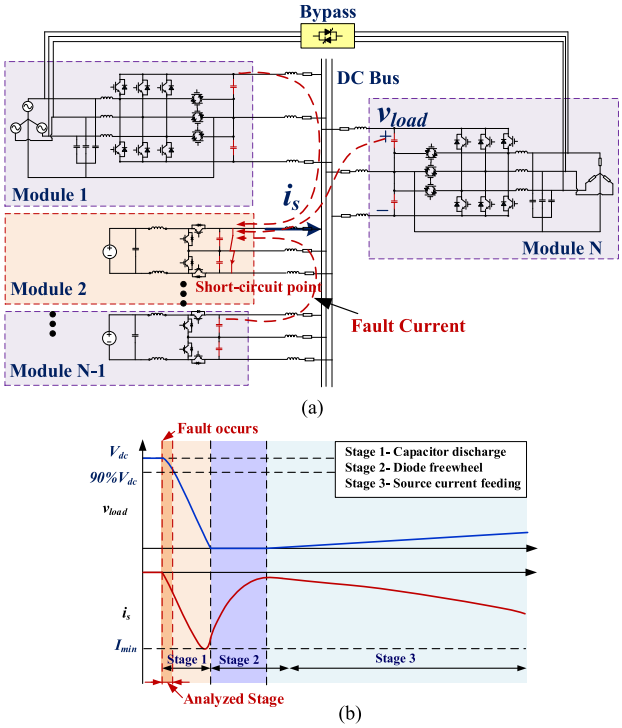

Fig. 3. Circuit model and the fault characteristic of Super-UPS. (a) Circuit model. (b) Characteristic of fault current and bus voltage.

to provide the power for the unbalanced three-phase load; thus, the dc bus needs the neutral point for the three-phase four-wire inverter. All energy sources and storage components are connected to a common dc bus through dc/dc or ac/dc converters. Since capacitors are installed in the dc port of converters, it results in the discharge current of the capacitors when the fault occurs in the dc port of converters. It can be seen in Fig. 3(a).

The diagram of the fault characteristic shown in Fig. 3(b) is obtained based on simulations. The detailed theoretical analysis of stages after short-circuit fault can be derived from [23] and [37]. According to the requirement of UPS, the fault should be cleared as fast as possible. Otherwise the drop in the dc-bus voltage will cause the interruption of the load power. Thus, the stage before the dc-bus voltage drops to 90% is analyzed. During this stage, the energy source module or storage module

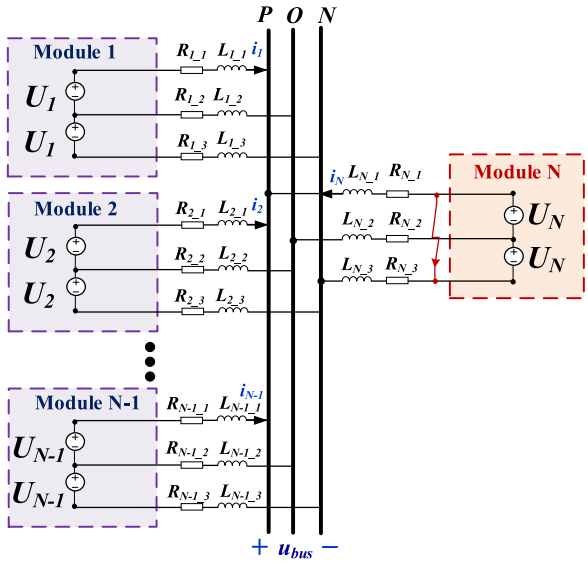

Fig. 4. Analytical model of the Super-UPS.

can be assumed as a constant-voltage source in order to simplify the analysis. The analytical fault model shown in Fig. 4 is used to analyze the characteristics of the fault current. It is assumed that the short-circuit fault occurs between the positive pole and negative pole in the dc port of Module N.

Equation (1) is derived according to the simplified model in Fig. 4. The fault current in the dc port of modules can be derived by solving (1). For higher than third-order equations, numerical solutions are used to solve them.

$$\begin{cases} (R_{1\_1}+R_{1\_3})i_1+(L_{1\_1}+L_{1\_3})\dfrac{di_1}{dt}+u_{\text{bus}}=2U_1 \\ (R_{2\_1}+R_{2\_3})i_2+(L_{2\_1}+L_{2\_3})\dfrac{di_2}{dt}+u_{\text{bus}}=2U_2 \\ \quad\bullet \\ \quad\bullet \\ \quad\bullet \\ (R_{N-1\_1}+R_{N-1\_3})i_{N-1}+(L_{N-1\_1}+L_{N-1\_3})\dfrac{di_{N-1}}{dt} \\ \quad +u_{\text{bus}}=2U_{N-1} \\ (R_{N\_1}+R_{N\_3})i_N+(L_{N\_1}+L_{N\_3})\dfrac{di_N}{dt}+u_{\text{bus}}=0 \\ i_1+\cdots+i_{N-1}+i_N=0 \end{cases} \tag{1}$$

where L_{i_1}, L_{i_2}, and L_{i_3} are the line inductances. R_{i_1}, R_{i_2}, and R_{i_3} are the line resistances. U_i is the output voltages of module i, and i_i is the fault current of module i. u_{bus} is the voltage of common point in dc bus.

C. Analysis of Fault-Current Direction

Based on the fault model shown in Fig. 4, a typical case is used to analyze the characteristics of fault current when

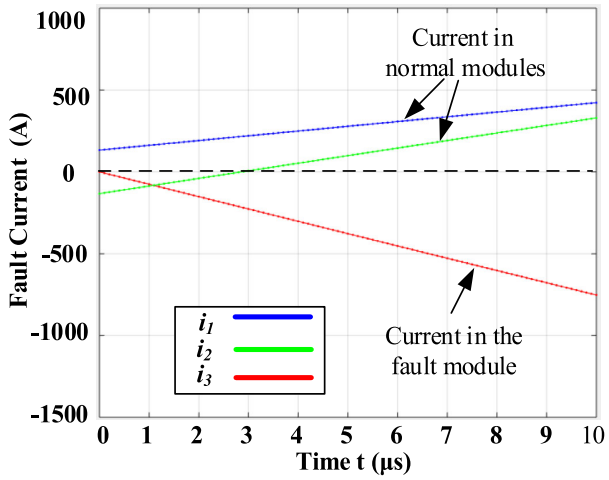

Fig. 5. Analytical results of the fault current.

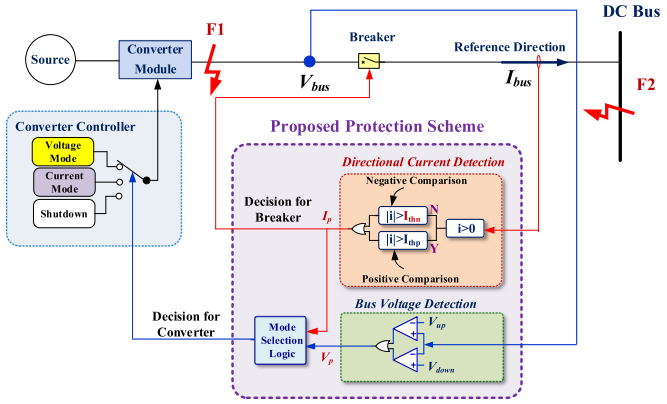

Fig. 6. Proposed protection scheme.

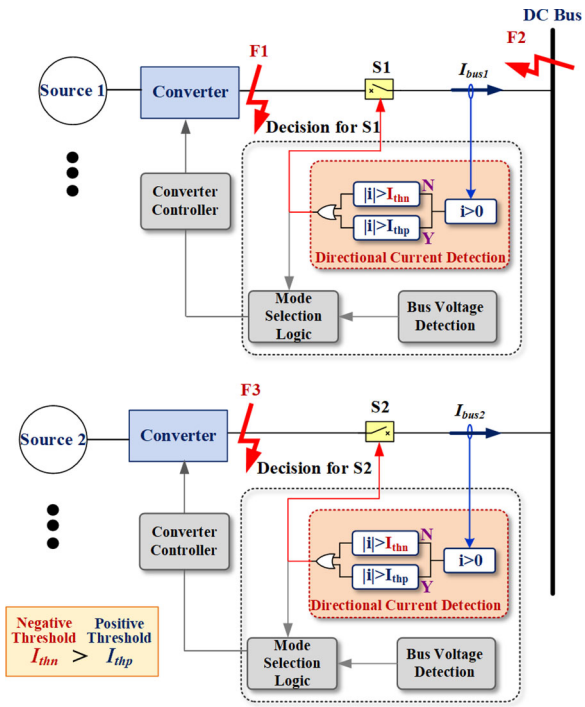

Fig. 7. Coordination of breakers for different fault locations.

N equals three. The parameters of cables used for calculation are listed in Table V.

The calculated result of fault current in the case is shown in Fig. 5.The initial condition is that Module 1 operates at the full load with a positive power flow. Module 2 is at the full load with a negative power flow. Module 3 is at no load. The power capacity of the modules is 100 kW, and dc-bus voltage is 750 V. Then, the rated current of the bus side is 133 A. So, the initial current of Modules 1, 2, and 3 are 133, –133, and 0 A, respectively. A more detailed analysis of fault current is provided in [38].

It is found that the initial value of the current has a little impact on the direction of fault current. Due to rapidly rising fault current, even though the initial direction of fault current i_2 in Module 2 is negative, it becomes positive within a very short period (2.8 μs). After that, the direction of fault current in the fault module is negative. The direction of fault current in all normal modules is positive. Besides, it can be proven that the derivative of the fault current in the fault module is always negative before the fault current reaches the minimum value, while the derivative of fault current in normal modules is positive. This characteristic of the fault-current direction is the basis to design the protection scheme.

III. Fast Fault-Protection Scheme Without Communication

A. Proposed Protection Scheme

The concept of protection scheme for Super-UPS is shown in Fig. 6. The proposed scheme generates the decisions for breakers and converters based on local measurements. First, the decisions for breakers depend on the directional current detection. According to the analysis of fault-current characteristic, the fault-current detection unit locates the fault based on the direction of the fault current. Different thresholds for two directions are set to distinguish the module fault and busbar fault. The threshold comparison for negative direction is used to trip the breaker when the module fault F1 occurs. The threshold comparison for positive direction is used to trip the breaker when the busbar fault F2 occurs. Second, the protection scheme coordinates with converters to ensure uninterruptible load power. It is based on the dc-bus voltage detection and the directional current detection. The decisions for converters are generated by mode-selection units. The converters change the modes according to the logic shown in Fig. 8. The protection scheme does not rely on any communication. A fast and robust protection is achieved, minimizing the fault affected area and ensuring uninterruptible load power.

The coordination of breakers for different fault locations is shown in Fig. 7, and the decisions for breakers are given in Table II. In order to achieve selective protection, the threshold for positive direction is higher than that for negative direction in the current-detection unit. Taking the fault F1 as an example, the fault current in S1 is negative, then S1 is tripped when current

TABLE II
DECISIONS FOR BREAKERS

Fault Location	Fault Current Direction in S1	Fault Current Direction in S2	Decision for S1	Decision for S2
F1	Negative	Positive	Trip*	No trip
F2	Positive	Positive	Trip**	Trip**
F3	Positive	Negative	No trip	Trip

*Negative threshold I_{thn} is reached, **Positive threshold I_{thp} is reached.

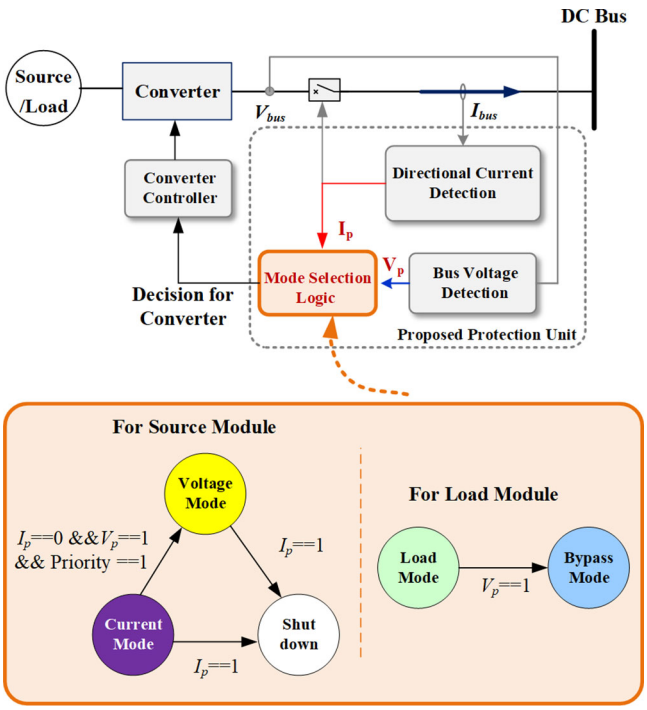

Fig. 8. Decision for converters in the protection scheme.

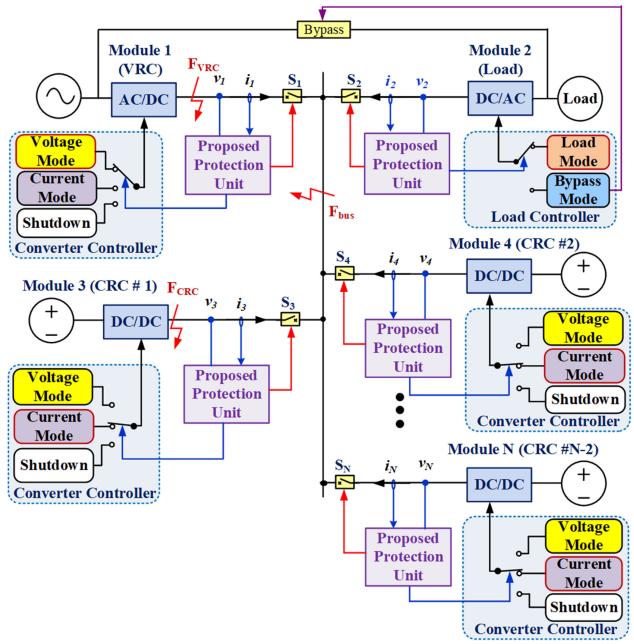

Fig. 9. Super-UPS with the proposed protection method.

reaches the negative threshold I_{thn}, while the fault current in S2 is positive. Since the positive threshold I_{thp} is higher than I_{thn}, the S2 is not tripped. According to Table II, it can be seen that only the faulty part is isolated based on the direction of fault current. The fault-affected area is minimized.

In order to achieve uninterruptible load power, it is necessary for the protection scheme to coordinate with converters in Super-UPS. The decision for converters is decided by the unit of mode-selection logic in Fig. 6. It relies on the fault detection signal I_p and the bus-voltage detection V_p. When dc-bus voltage is lower than V_{down} or higher than V_{up}, V_p turns to "1." When the fault is detected by directional current-detection unit, I_p turns to "1." The detailed threshold setting rule is analyzed in Section III-B. The logic of mode selection is given in Fig. 8. The mode-selection logic for the source module and the load module is different. For the source module, the converter changes its mode among voltage mode, current mode and shutdown. It should be noticed that the current-mode modules have priorities to change their modes to voltage mode when voltage-mode module fault occurs. For the load module, the load converter changes its mode between load mode and bypass mode. The coordination of protection is also based on local measurement without any message exchange with other modules.

The Super-UPS with proposed protection scheme is shown in Fig. 9. As a compact power supply, Super-UPS is master-slave system. There is a bus voltage regulation converter (VRC) Module 1, a load inverter Module 2 and multiple current regulation converters (CRCs) Module 3 ~ N. Module 3 is preconfigured as CRC #1, which has the highest priority as the backup module of VRC. The bypass switches are controlled by the load module.

The operation of the protection scheme for different fault locations is analyzed from Figs. 10–12. The CRC fault F_{CRC}, VRC fault F_{VRC} and busbar fault F_{bus} are analyzed in detail. The decisions for breakers and converters under short-circuit fault F_{CRC} are shown in Fig. 10. In Fig. 10(a), when the short-circuit fault occurs in Module 3 (CRC), the fault current in Module 3 is negative, while the fault current in other modules is positive. Since the threshold for negative direction I_{thn} is set lower than threshold for positive direction I_{thp}, the S_3 is tripped first. While, the SSCBs connected to other modules are not tripped. The selectivity of protection is achieved, and the area affected by the fault is minimized. After the Module 3 is isolated by SSCBs based on the direction of fault current, the controller of Module 3 shuts down the converter by the mode-selection logic unit. The controllers of other modules do not need to change.

If short-circuit fault F_{VRC} occurs in Module 1 (VRC), then Module 1 is isolated by the SSCB based on directional current detection as shown in Fig. 11(a). However, in this situation, the system loses the bus-voltage regulator VRC. The controller of Module 3 (CRC #1) detects the dc-bus voltage. When the bus voltage exceeds the bus voltage threshold of the source module $V_{\text{down}(s)}$, the controller of Module 3 changes its mode from the current-control mode to the voltage-control mode based on the

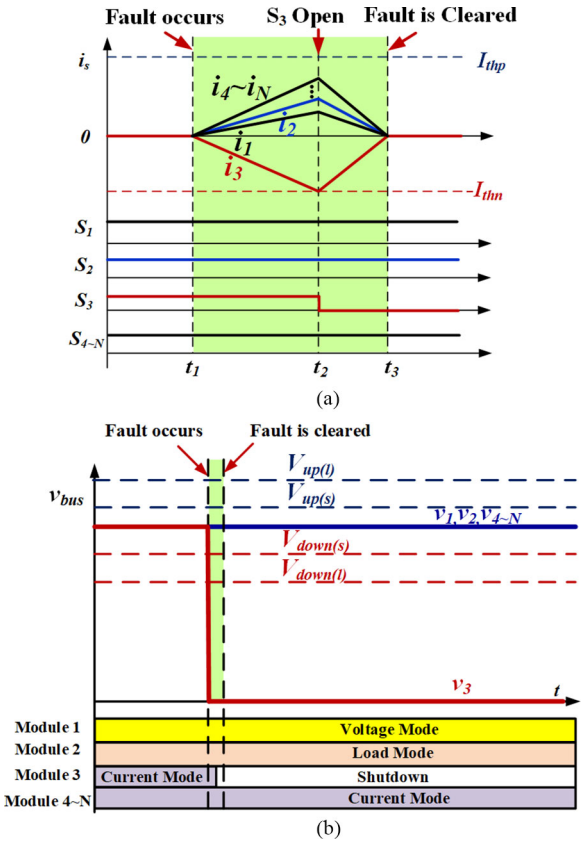

Fig. 10. Operation of the protection when module CRC #1 fault occurs. (a) Decisions for breakers. (b) Decisions for converters.

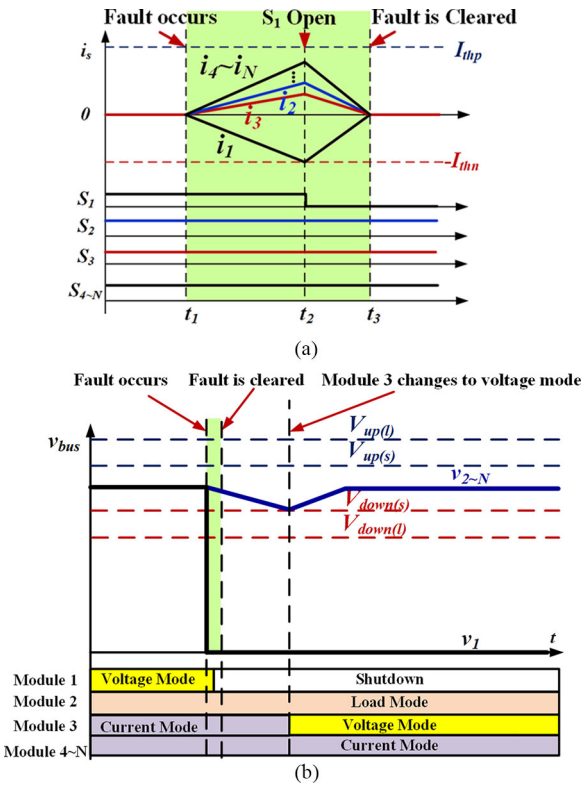

Fig. 11. Operation of the protection when module VRC fault occurs. (a) Decisions for breakers. (b) Decisions for converters.

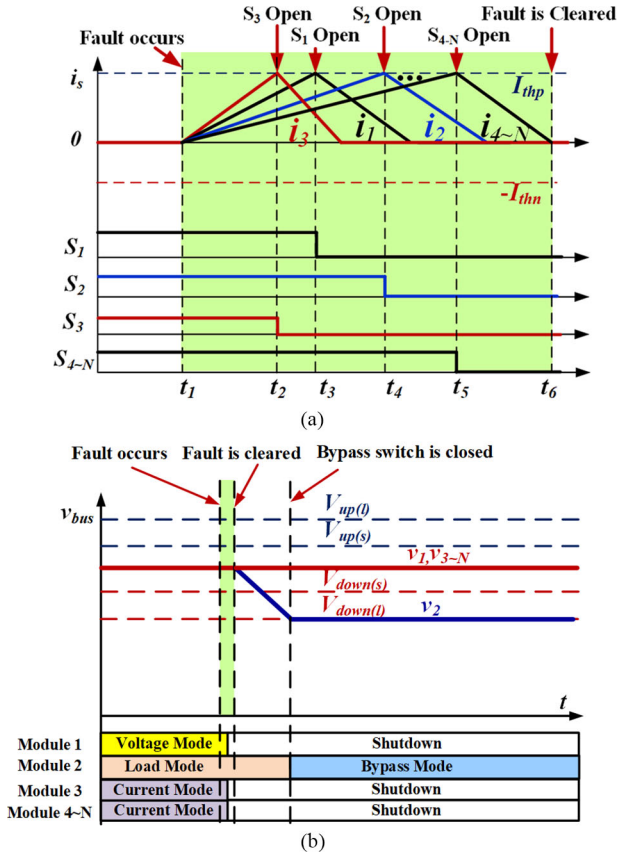

Fig. 12. Operation of the protection when a bus fault occurs. (a) Decisions for breakers. (b) Decisions for converters.

mode-selection logic. Module 3 becomes the new VRC to regulate the bus voltage. The controllers of other modules do not need to change. The decisions for converters are shown in Fig. 11(b).

If a short-circuit fault F_{bus} occurs in the dc busbar, the protection strategy operates to avoid the damage of SSCBs and the components of the converter module. In Fig. 12(a), the fault current in all modules is positive when a bus fault occurs. The thresholds for the positive direction of all modules are reached. Then, all modules are isolated by SSCBs. Since Module 2 (load module) loses the input power, the bus voltage of Module 2 begins to decrease. When the dc-bus voltage decreases to the bus voltage threshold of the load module $V_{\text{down}(l)}$, the bypass switch is closed by Module 2. The branch of bypass provides the power for the load. It can be seen that the load is uninterruptible when short-circuit fault occurs in the dc busbar. The decisions for converters are shown in Fig. 12(b).

If one breaker malfunctions, the backup protection is necessary to protect the power devices of SSCB and dc capacitors in the fault paths. If S_3 malfunctions when the fault F_{CRC} occurs in Module 3, then S_1, S_2 and $S_4 \sim S_N$ will provide the backup protection. The thresholds for positive direction of all modules will be reached when S_3 malfunctions. When all breakers are tripped, the fault current is blocked. Since Module 2 loses the input power, then Module 2 changes the mode from load mode to bypass mode when the dc-bus voltage decreases to the threshold $V_{\text{down}(l)}$. The bypass provides the power for the load.

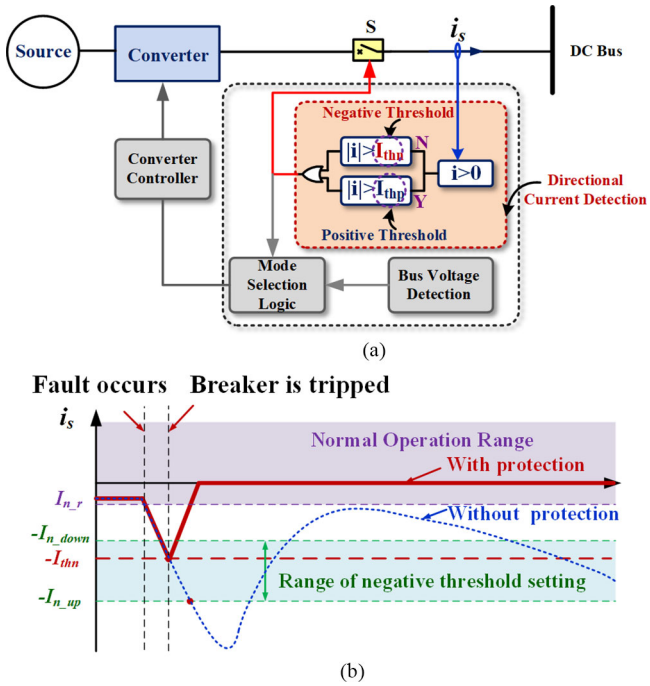

Fig. 13. Negative threshold setting of protection scheme. (a) Thresholds in directional fault current detection. (b) The range of negative threshold.

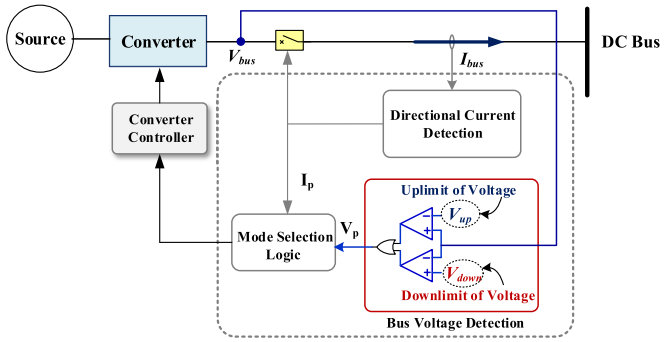

Fig. 14. Voltage threshold setting of protection scheme.

B. Threshold Setting for the Proposed Protection Scheme

1) Current Threshold Setting for Negative Direction: The threshold setting for two directions is critical for coordination of SSCBs. The threshold setting for negative direction is used to trip the SSCBs connected with the fault module. The negative threshold should fulfill the requirement of (2). The range of threshold is shown in Fig. 13(b). The types of sources should be taken into account to design the threshold for negative direction. The current in normal mode of the unidirectional source is always positive, and the negative rated current I_{n_r} of the unidirectional source is set to zero.

$$\begin{cases} I_{n\_\text{down}} = \max\left\{-3I_{r\_n}, |I_{dy}|, I_{\text{sam\_down}}\right\} \\ I_{n\_\text{up}} = \min\left\{|I_{90\%}|, I_{\text{cap\_max}}, I_{pd\_\text{max}}\right\} - t_d \cdot k_{i\_\text{max}} \\ I_{n\_\text{down}} < I_{thn} < I_{n\_\text{up}} \end{cases} \quad (2)$$

where I_{dy} is the maximum transient current when the module starts or load steps. I_{r_n} is the negative rated current. $I_{\text{sam\_down}}$ is the down limit of threshold caused by measurement method. This content is analyzed in Section III-C. The down limit of threshold using the least-square (LS) method is derived as (12). $I_{\text{cap\_max}}$ is the maximum current the capacitors can handle. It depends on the *dv/dt* limit of capacitors. $I_{\text{pd\_max}}$ is the maximum current that the breaker allows. Normally, the $I_{\text{pd\_max}}$ is three times of rated current of power device if SSCB is applied. k_{i_max} is the maximum slope of fault current in the system. t_d is the time delay of protection. $I_{90\%}$ is the fault current value when the dc-bus voltage of the load module drops to 90% of the rated bus voltage.

In order to avoid malfunctions, the reliability factors K_{rel1} and K_{rel2} can be introduced. Equation (2) can be rewritten as follows:

$$\begin{aligned} &\left[\max\left\{-3I_{r\_n}, |I_{dy}|, I_{\text{sam\_down}}\right\}\right] K_{\text{rel1}} < I_{\text{thn}} \\ &< \left[\min\left\{|I_{90\%}|, I_{\text{cap\_max}}, I_{\text{pd\_max}}\right\} - t_d \cdot k_{i\_\text{max}}\right] K_{\text{rel2}}. \end{aligned} \quad (3)$$

2) Current Threshold Setting for Positive Direction: The threshold setting for positive direction has two functions. One is providing a backup protection when SSCBs are installed in the fault module malfunction. The other one is tripping all SSCBs to isolate the dc busbar fault.

Compared with the threshold for negative direction, the positive threshold setting does not depend on the type of sources. Based on the requirement of coordination of SSCBs, the positive threshold of module *i* should be larger than the negative thresholds of all other modules. The range of positive threshold is given in the following:

$$\begin{aligned} &\max\{|I_{\text{thn}(1)}|, \ldots, |I_{\text{thn}(i-1)}|, |I_{\text{thn}(i+1)}|, \ldots, |I_{\text{thn}(N)}|\} \\ &< I_{\text{thp}(i)} (1 \le i \le N) \end{aligned} \quad (4)$$

where $I_{\text{thp}(i)}$ and $I_{\text{thn}(i)}$ are the positive threshold and the negative threshold of module *i*, respectively.

3) Voltage Threshold Setting for Mode-Selection Unit: The mode selection of the converter is based on the bus-voltage detection. In Fig. 14, when the dc-bus voltage is lower than V_{down} or higher than V_{up}, the mode-selection unit is tripped to change the mode of converters based on the selection logic in Fig. 8. The ranges of V_{down} and V_{up} are given in the following, respectively,

$$\begin{cases} \dfrac{2\sqrt{2}V_{\text{load\_RMS}}}{m_{\text{inv}}} < V_{\text{down}} < (1-p)V_r \\ (1+p)V_r < V_{\text{up}} < V_s \end{cases} \quad (5)$$

where m_{inv} is the amplitude-modulation ratio of the load inverter, $V_{\text{load\_rms}}$ is the phase voltage of load inverter, p is the maximum fluctuation of bus voltage at the normal state, and V_s is the maximum safe voltage for converters. As shown in (6), it should be noticed that the threshold voltage $V_{\text{down}(l)}$ for the load module should be lower than the threshold $V_{\text{down}(s)}$ for CRC. Otherwise, when VRC fault occurs in Fig. 11, the load module may change to bypass mode by mistake. Similarly,

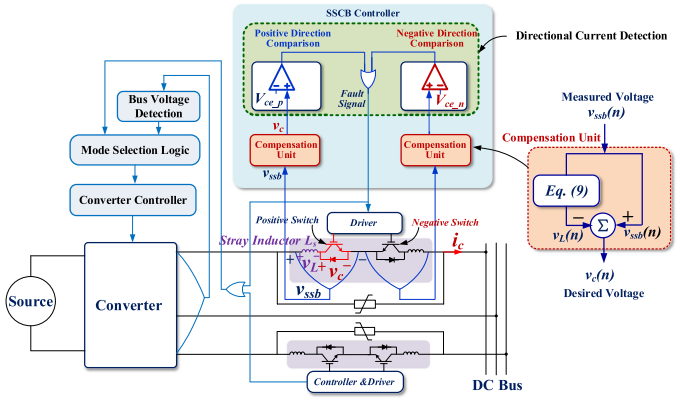

Fig. 15. Improved current measurement method for proposed protection scheme.

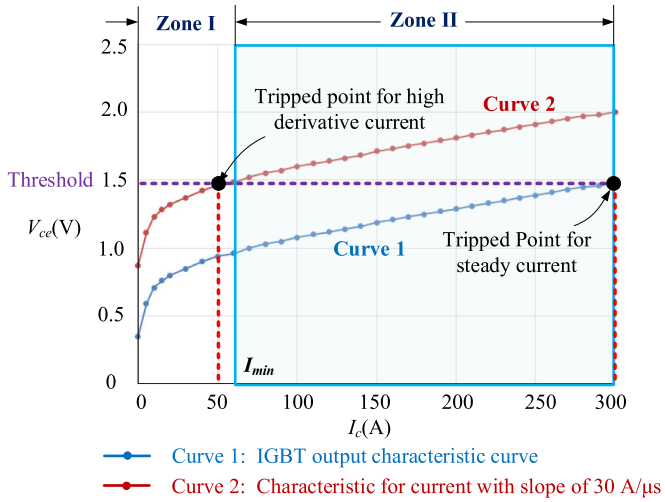

Fig. 16. Effect of stray inductor on the current measurement.

$V_{\mathrm{up}(l)}$ for load module should be higher than the threshold $V_{\mathrm{up}(s)}$ for CRC.

$$\begin{cases} V_{\mathrm{down}(l)} < V_{\mathrm{down}(s)} \\ V_{\mathrm{up}(l)} > V_{\mathrm{up}(s)} \end{cases} \tag{6}$$

C. Improved Fault-Current Measurement Method for Accurate Operation of Protection Scheme

Due to the requirement of fast isolation, SSCBs need to be installed in the dc port of modules in the Super-UPS. The realization of the proposed protection scheme with SSCBs is shown in Fig. 15. The directional fault current detection can be easily implemented into SSCB by setting collector–emitter voltage thresholds for the positive switch and negative switch, respectively. However, there is a large measurement error for the traditional current-measurement method based on the voltage drop of SSCB when the derivative of the fault current is high.

Owing to the existence of stray inductor L_s in the insulated gate bipolar transistor (IGBT) module in Fig. 15, the measured v_{ssb} voltage consists of the desired IGBT chip voltage v_c and stray inductor voltage drop v_L. The stray inductor voltage is directly proportional to the derivative of current. For the same value of current with different derivatives, the measured voltage of SSCB is quite different. In Fig. 16, assuming that the current derivative is 30 A/μs, which is a typical value in Super-UPS and the stray inductance is 20 nH, the threshold for steady current is 300 A. The same threshold will be reached when current is 50 A with derivative of 30 A/μs.

An improved measurement method is proposed to eliminate the effect of stray inductor on the measurement. In the proposed method, the voltage drop of SSCB is sampled by the digital controller, and the extra voltage caused by stray inductor is eliminated by the compensation unit shown in Fig. 15. The compensated results are sent to a comparison unit to trip the breaker. The compensation unit is based on the linear zone of IGBT output characteristic curve, which is shown as Zone II of Curve 1 in Fig. 16. I_{min} is defined as the minimum current of Zone II. When the current is larger than I_{min}, the relationship between voltage V_{ce} and current I_c of IGBT is linear. It can be expressed as follows:

$$V_{ce}(I_c) = kI_c + b \quad (I_c \geq I_{\mathrm{min}}) \tag{7}$$

where k and b are the fitting coefficients of IGBT output characteristic curve.

According to Fig. 15 and (7), the following equation is derived with the assumption of the constant current derivative during the short analyzed period:

$$\begin{cases} v_L(t) = \dfrac{L_s}{k}\dfrac{dv_{\mathrm{ssb}}(t)}{dt} \\ v_c(t) = v_{\mathrm{ssb}}(t) - \dfrac{L_s}{k}\dfrac{dv_{\mathrm{ssb}}(t)}{dt} \end{cases} \tag{8}$$

where L_s is stray inductance of SSCB and k is the parameter in (7).

According to (8), the voltage drop of the stray inductors V_L and the desired IGBT chip voltage V_c is related to the derivative of the measured voltage drop of SSCB V_{ssb}. Since the derivative calculation is sensitive to the sampling error, a LS method is applied in order to reduce the measurement error. In the LS method, adjacent three points are used to calculate the derivative, which is shown in Fig. 17. After discretizing (8), the voltage drop of the stray inductors V_L can be expressed in (9), and the desired V_c voltage is shown in (10). T_s is the sampling period.

$$v_L(n) = L_s \frac{v_{\mathrm{ssb}}(n) - v_{\mathrm{ssb}}(n-2)}{2kT_s} \tag{9}$$

$$v_c(n) = v_{\mathrm{ssb}}(n) - v_L(n) = \left(1 - \frac{L_s}{2kT_s}\right) v_{\mathrm{ssb}}(n) + \frac{L_s}{2kT_s} v_{\mathrm{ssb}}(n-2) \tag{10}$$

In (10), it can be seen that the calculation result of V_c depends only on voltage drop of SSCB, sampling period, and inductance of stray inductor. It does not use the information of the current. The calculated result V_c is compared with the threshold to trip the SSCB. According to the IGBT output characteristic curve in Fig. 16, the threshold of V_c can be derived by the desired

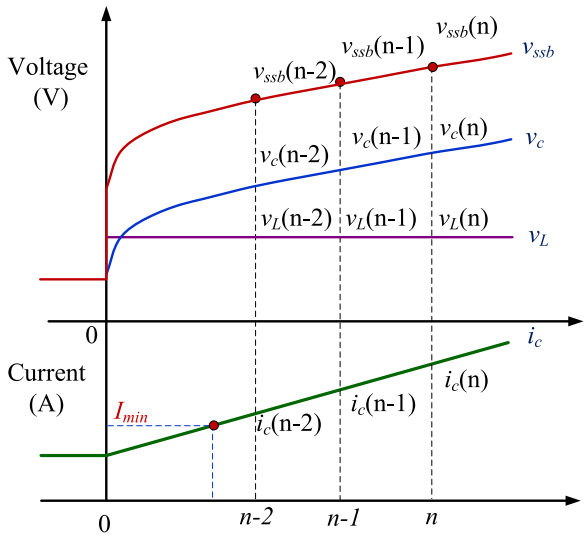

Fig. 17. Calculation of stray inductor voltage for the improved measurement method.

fault-current threshold. The threshold $I_{\text{th}n}$ and $I_{\text{th}p}$ shown in Fig. 13 can be converted to the V_{ce_n} and V_{ce_n} of SSCB using (7). The V_{ce_n} and V_{ce_p} are derived as given in the following:

$$\begin{cases} V_{ce\_n} = kI_{\text{th}n} + b \\ V_{ce\_p} = kI_{\text{th}p} + b. \end{cases} \tag{11}$$

It should be noticed that the current at the first valid point used for calculation should be larger than I_{min}. Thus, the protection threshold settings should meet the requirement of (12). Otherwise, the calculated results used for tripping the SSCB will be invalid.

$$I_{\text{th}n/\text{th}p} \geq I_{\text{min}} + 2T_s k_I \tag{12}$$

where k_I is the derivative of fault current.

D. Comparison Between the Proposed Protection Method and Conventional Methods

A comparison between the proposed method and other methods is provided in Table III. The fault-clearing time for different types of faults and the reliability of load power are compared. The data of the proposed method are based on the experimental results. For the directional overcurrent protection method [35], the fault detection only responds for one direction of fault current. The breakers are tripped only for the module fault. It does not operate for busbar fault. Besides, the load is interrupted when the fault occurs in the common bus. The handshaking method [9] does not rely on communication, and it improves the robustness of protection. However, all converters are shut down after the fault is detected. The loads on the healthy buses are interrupted temporarily. For the directional comparison protection [23] and hybrid protection method [17], [33], the protection speed may not meet the requirement of protection in the compact power supply due to the dependence on communication. It will cause the interruption of load power.

The proposed scheme has three metrics for the compact and uninterruptible power supply system: 1) detecting both module faults and busbar faults locally and quickly; 2) ensuring the uninterruptible load power without assistance of communication; and 3) accurate and reliable operation of protection for rapidly rising fault current by the improved measurement method. Thus, the protection speed and the reliability of load are improved.

IV. Experimental Results

A. Prototype of Super-UPS

The prototype of a Super-UPS is built to verify the proposed protection scheme. In the prototype, there are two kinds of standard converter modules, bidirectional ac/dc module and bidirectional dc/dc module. The SSCBs are installed in the dc-bus side of the converter modules. The metal oxide varistors (MOVs) are used to protect the SSCBs. The prototype of the Super-UPS is shown in Fig. 18. The parameters of the standard converter modules and SSCBs are shown in Table IV. The architecture of the system is shown in Fig. 19. The line parameters among modules are given in Table V.

B. Accuracy Test of Fault-Current Threshold Setting

The accuracy test of the proposed measurement method with stray inductor voltage compensation is shown in Fig. 20. The sampling frequency of digital controller is 1 MHz. The theoretical down limit and up limit are calculated based on the time delay of digital processing and marked in Fig. 20(a). It can be seen that the three test results are within the theoretical limits. The error between the trip current and threshold is shown in Fig. 20(b).

C. Verification of Protection Scheme

The Super-UPS is designed modularly and configured flexibly. In Fig. 19, three modules are configured to verify the protection scheme of the system. Module 1 (M1) regulates the bus voltage. Module 2 (M2) is the load. Module 3 (M3) controls the output power. The bypass is installed to connect the utility and load. A 1700 V/2400 A IGBT is used to simulate the short-circuit fault point. MOV is also used to protect the IGBT at the short-circuit point. The threshold setting of the module is given in Appendix A.

The protections for different fault locations are verified. The fault locations include CRC, VRC, and the dc busbar. First, the fault occurs in the bus side of CRC M3. The protections under different operation points are tested. In the test, the rated power of load is 30 kW. In Fig. 21, the initial powers of M1, M2, and M3 are 20, –20, and 0 kW, respectively. From Fig. 21(a), it can be seen that there is no change of load current and input current of normal module when short-circuit fault occurs. The dc-bus voltage of load M2 is also kept constant. During the fault, the load is not interrupted. In Fig. 21(b), the characteristic of fault-current direction is shown clearly. The fault current flowing through the SSCB S3 connected to fault module M3 is negative. The fault current in normal modules M1 and M2 increases positively. The direction of fault current is used to

TABLE III
COMPARISON BETWEEN THE PROPOSED METHOD AND OTHER METHODS

Methods	Clearing Time for Module Faults	Clearing Time for Bus Faults	Assistance of Communication	Uninterruptible Load Power	System Topology
Directional overcurrent protection method in [35]	3 ms	Unhandled	No	No	Radial
Directional comparison protection method in [23]	Not mentioned	2 ms	Yes	Yes*	Meshed
Handshaking method in [9]	Not mentioned	500 ms	No	Temporary Interruption	Meshed
Combination of differential and overcurrent protection in [33]	5 ms	1 ms	Yes	Yes*	Meshed
Hybrid protection method in [17]	70 μs	100 μs	Yes	No	Radial
Proposed protection method	13 μs	22 μs	No	Yes	Radial

*For the compact power-supply system, it may cause temporary interruption of load due to the communication delay.

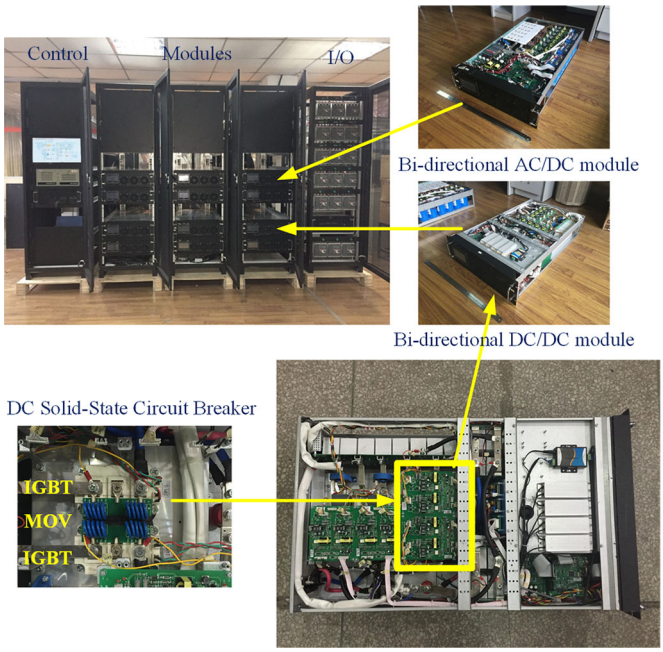

Fig. 18. Prototype of Super-UPS and SSCBs.

TABLE IV
SPECIFICATIONS OF THE MODULES IN SUPER-UPS

Standard Bi-directional AC/DC		Standard Bi-directional DC/DC	
Item	Value	Item	Value
Power capacity	100 kW	Power capacity	30 kW
Input voltage	380 V	Input range	200-400 V
Input inductor	0.38 mH	Input inductor	0.32 mH
Input capacitor	200 μF	Input capacitor	400 μF
Output capacitor	4400 μF	Output capacitor	400 μF
Rated bus-side voltage	±375 V	Rated bus-side voltage	±375 V
Rated current in bus-side	133 A	Rated current in bus-side	40 A
SSCB			
IGBT model number	FF450R12KE4_E	MOV model number	EPCOS S20K300E2
IGBT rated voltage	1200 V	MOV varistor voltage	470 V
IGBT rated current	450 A		

locate the fault module. The threshold for negative direction is set to be 120 A. Owing to the time delay in the protection, the final turn-off fault current of the SSCB in Module 3 is –180 A. During the fault, there is no dip in the dc-bus voltage of M2. The fault is cleared within 11 μs.

The protection waveforms under another initial state are shown in Fig. 22. The initial powers of M1, M2, and M3 are 0, –20, and 20 kW, respectively. Before the fault occurs, M1 regulates the dc-bus voltage and M3 provides the load power. It can be seen that M3 is isolated after the fault M1 provides the load power. In Fig. 22(b), the turn-off fault current in fault module is –178 A. The fault is cleared within 13 μs. It also shows that the load is not interrupted in this situation.

Next, the fault location is in the bus side of VRC M1. When the fault occurs in M1, the waveforms of protection are shown in Fig. 23. M1 is isolated by the SSCB when the fault current reaches the negative threshold. The system loses VRC, and the dc-bus voltage begins to decrease after M1 is isolated. M3 detects the dc-bus voltage, and its operation mode changes from current-control mode to bus-voltage control mode when the bus voltage drops to the threshold of 720 V. It can be seen that the load is not interrupted during the transferring. The initial current direction of modules and the fault condition in Fig. 24 are the same as Fig. 23; however, the load level is half. Similarly, the load is not interrupted during the fault.

Third, the fault location is in the dc busbar. When the fault occurs in the dc bus, all SSCBs are tripped and all modules are isolated. The fault is cleared within 22 μs. The load inverter detects the dc-bus voltage and turn ON the bypass switches when bus voltage drops to the threshold of 700 V. The bypass provides the load power after the fault is isolated. From Fig. 25(a), it can be seen that the load is not interrupted when the fault occurs in the dc bus.

D. Sensitivity Discussion of Protection Scheme

Based on the experimental scheme shown in Fig. 19, the sensitivity of protection scheme under different conditions is tested, and the experimental results are shown in Fig. 26. Multiple operation conditions including load connecting, load disconnecting, overcurrent fault in load side, and utility failure at different load levels are considered. In Fig. 26, it can be seen that there is no false tripping of protection for the conditions of load connecting, load disconnecting, and utility failure. For the overcurrent fault in load side, there is no false tripping when the overcurrent

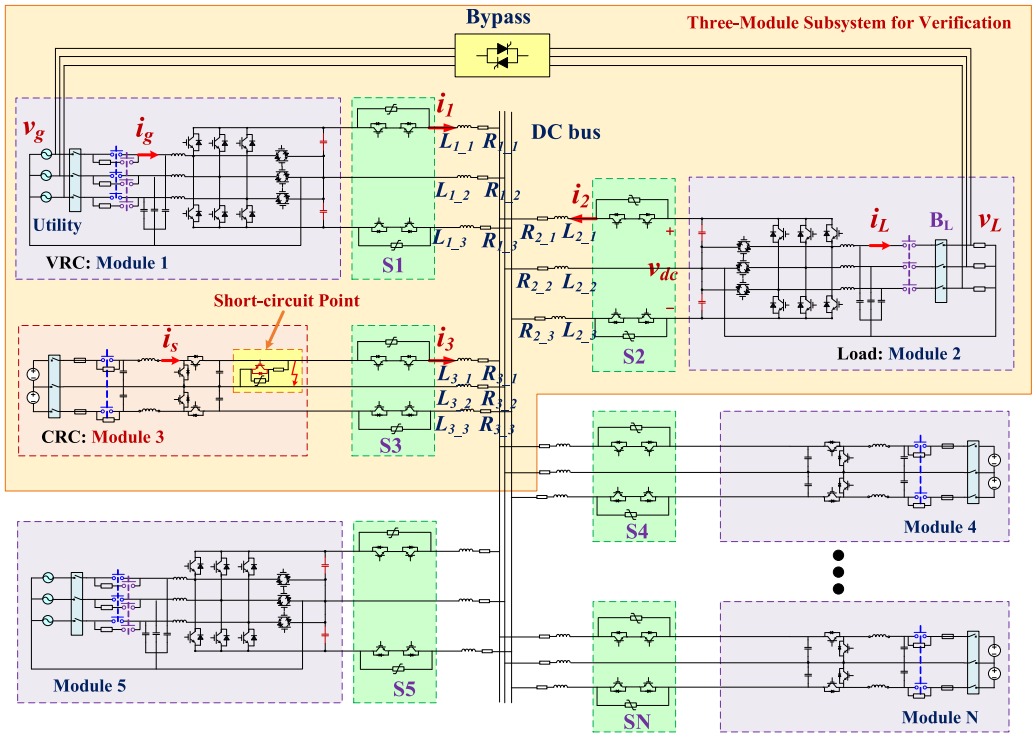

Fig. 19. Architecture of Super-UPS.

TABLE V
CABLE PARAMETERS OF VERIFICATION

Module 1		Module 2	
Module type	Standard AC/DC	Module type	Standard AC/DC
Line inductor L_{1_1}	3.8 μH	Line inductor L_{2_1}	2.2 μH
Line inductor L_{1_2}	1.8 μH	Line inductor L_{2_2}	1.3 μH
Line inductor L_{1_3}	3.2 μH	Line inductor L_{2_3}	2.2 μH
Line resistor R_{1_1}	4.8 mΩ	Line resistor R_{2_1}	2.8 mΩ
Line resistor R_{1_2}	2.5 mΩ	Line resistor R_{2_2}	1.6 mΩ
Line resistor R_{1_3}	4.4 mΩ	Line resistor R_{2_3}	2.8 mΩ
Module 3			
Module type	Standard DC/DC	Line resistor R_{3_1}	6.5 mΩ
Line inductor L_{3_1}	5.0 μH	Line resistor R_{3_2}	1.7 mΩ
Line inductor L_{3_2}	1.3 μH	Line resistor R_{3_3}	2.9 mΩ
Line inductor L_{3_3}	2.2 μH		

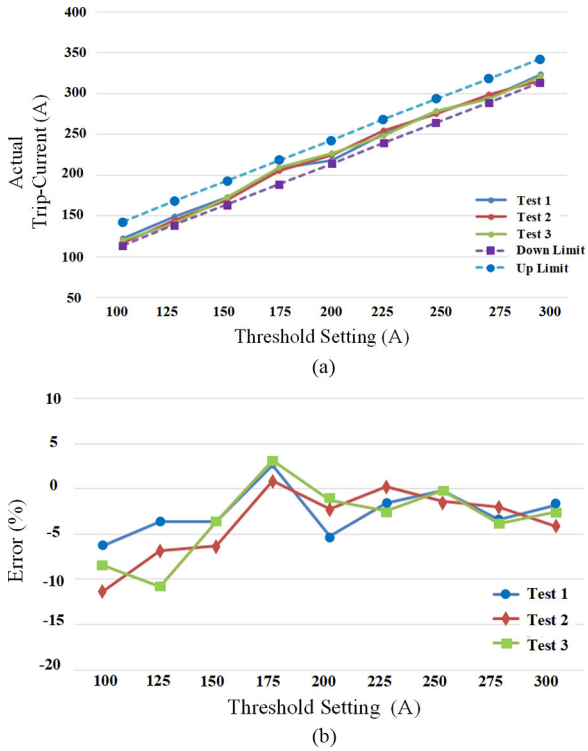

Fig. 20. Three test results of trip-current of SSCB (@ current derivative 29 A/μs). (a) Absolute value of trip current. (b) Error of the trip current.

threshold of load side is 1.5 times of the rated load current. However, if the overcurrent threshold of load side is larger than twice of the rated load current, the false tripping of bus-side SSCBs occurs. If there is a special need for the system to operate at more than twice of the rated load current, the threshold of protection scheme needs to be redesigned. For the short-circuit faults in bus side, Fig. 26 shows that the protection is tripped accurately. The difference between the trip current and the turn-OFF current is caused by the protection delay and high derivative of fault current. In addition, the fault current is large enough to trip the threshold when the short-circuit fault occurs in bus side. The influence of line impedance on fault current is given in Appendix B.

The experimental results at full load are shown in Fig. 27. In Fig. 27(a), the breaker of load side is closed at t_1, and a 30-kW load is connected. The maximum transit current flowing through the SSCB S2 in bus side is 58 A, which is lower than the threshold 120 A. In Fig. 27(b), the load is disconnected

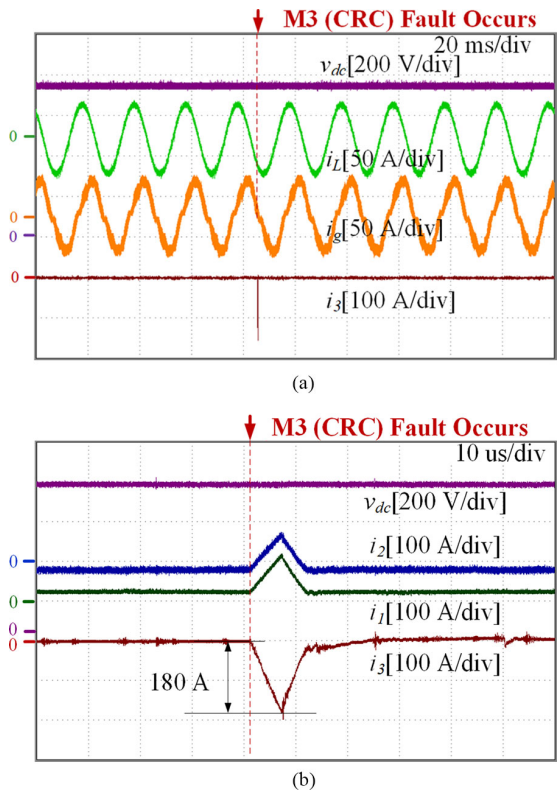

Fig. 21. Protection waveforms when a fault occurs in CRC M3 (M1: 20 kW, M2: –20 kW, M3: 0 kW). (a) Overall protection waveforms. (b) Detailed waveforms at the fault time.

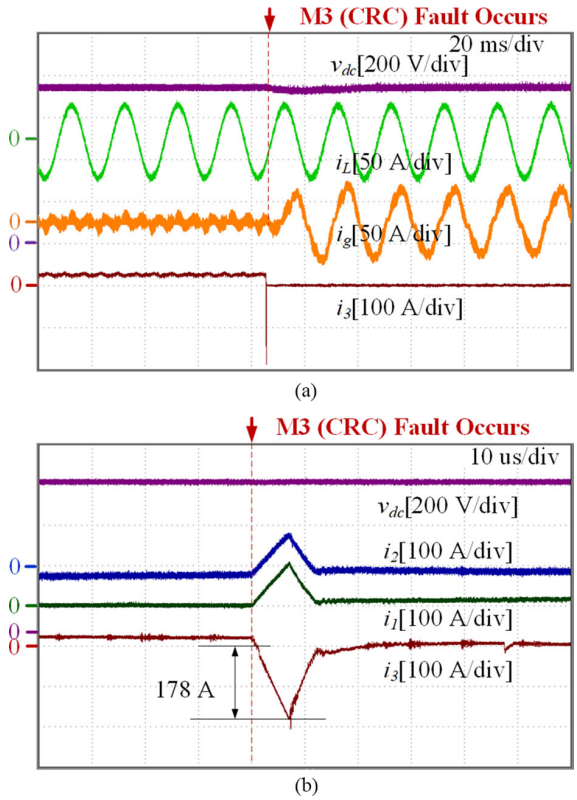

Fig. 22. Protection waveforms when a fault occurs in CRC M3 (M1: 0 kW, M2: –20 kW, M3: 20 kW). (a) Overall protection waveforms. (b) Detailed waveforms at the fault time.

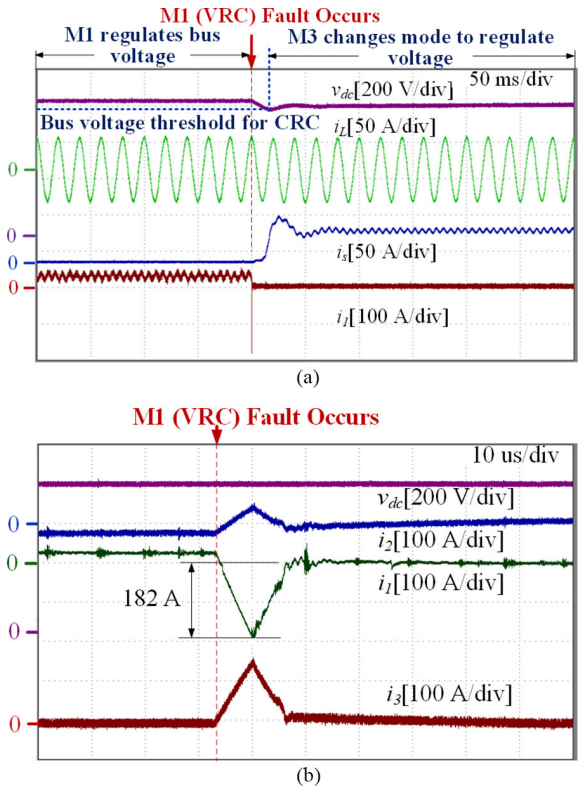

Fig. 23. Protection waveforms when a fault occurs in VRC M1 (M1: 20 kW, M2: –20 kW, M3: 0 kW). (a) Overall protection waveforms. (b) Detailed waveforms at the fault time.

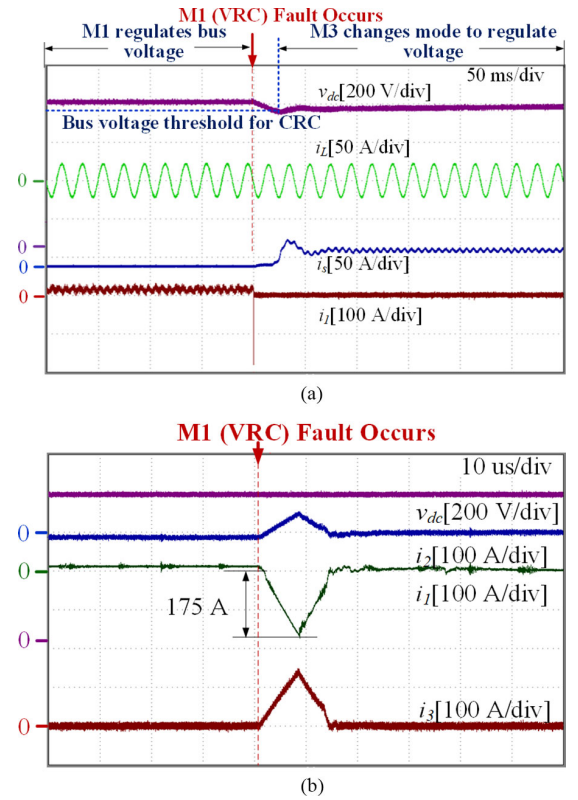

Fig. 24. Protection waveforms when a fault occurs in VRC M1 (M1: 10 kW, M2: –10 kW, M3: 0 kW). (a) Overall protection waveforms. (b) Detailed waveforms at the fault time.

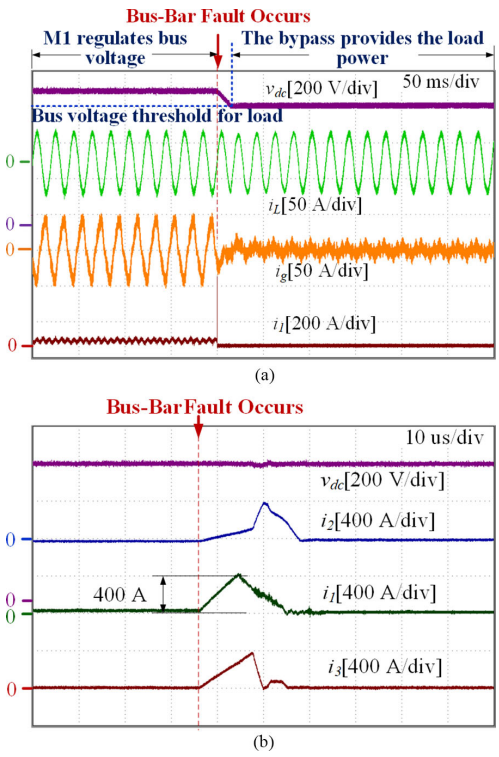

Fig. 25. Protection waveforms when a fault occurs in dc busbar (M1: 20 kW, M2: –20 kW, M3: 0 kW). (a) Overall protection waveforms. (b) Detailed waveforms at the fault time.

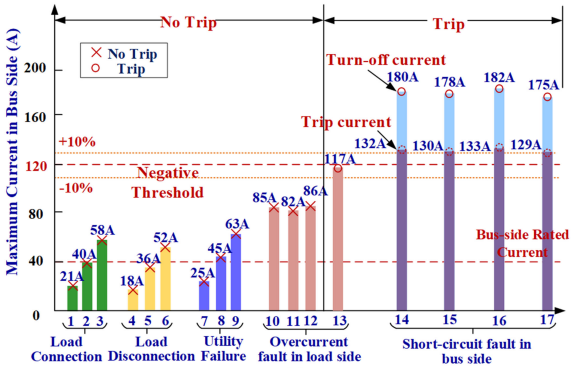

(a)

Condition	Index	Description
Load Connection	1	1/3 Load
	2	2/3 Load
	3	Full Load
Load Disconnection	4	1/3 Load
	5	2/3 Load
	6	Full Load
Utility Failure	7	1/3 Load
	8	2/3 Load
	9	Full Load
Overcurrent fault in load side	10	1/3 Load, Overcurrent threshold: 1.5x I_r*
	11	2/3 Load, Overcurrent threshold: 1.5x I_r
	12	Full Load, Overcurrent threshold: 1.5x I_r
	13	Full Load, Overcurrent threshold: 2x I_r
Short-circuit fault in bus side	14	CRC Fault 1 (Fig. 21)
	15	CRC Fault 2 (Fig. 22)
	16	VRC Fault 1 (Fig. 23)
	17	VRC Fault 2 (Fig. 24)

*I_r:rated load current

(b)

Fig. 26. Experiment results for sensitivity analysis. (a) Results of sensitivity tests. (b) Description of the cases.

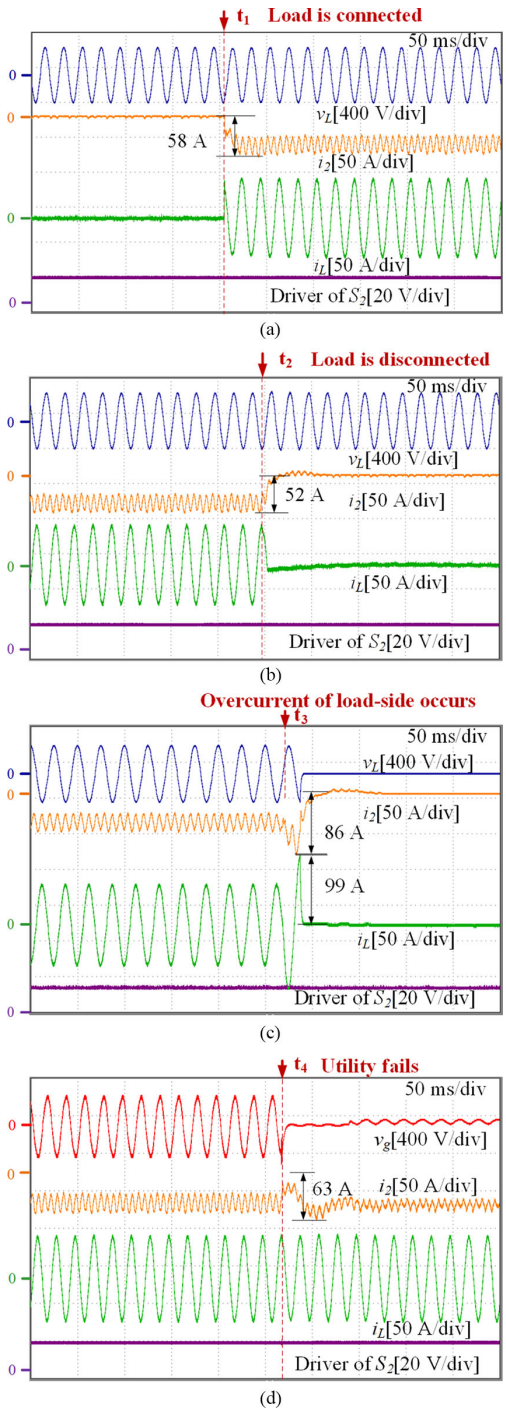

Fig. 27. Sensitivity of protection scheme under different conditions. (a) Sensitivity of load connecting. (b) Sensitivity of load disconnecting. (c) Sensitivity of overcurrent fault in load side. (d) Sensitivity of utility failure.

at t_2. Fig. 27(c) shows the waveform under the condition of overcurrent fault in load side. Before the fault, the load power is 30 kW. The overcurrent fault of load side occurs at t_3, and the load current increases dramatically to the overload threshold of load side (1.5 times of the rated load current). The sensitivity under utility failure is tested in Fig. 27(d). The utility fails at t_4, and M1 shuts down while M3 begins to provide the power of load. There is no false tripping of SSCBs under these conditions.

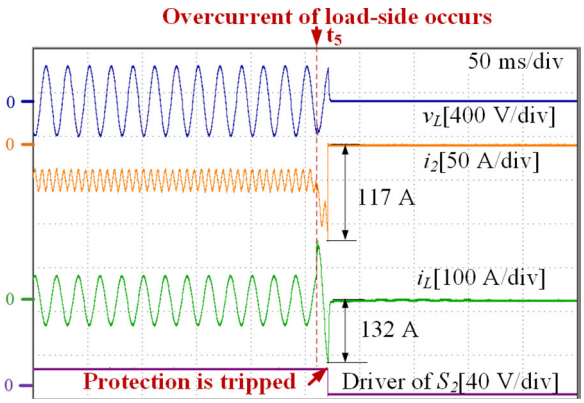

Fig. 28. False tripping of protection at overcurrent fault (2x rated current) in load side.

In addition, the false tripping of protection at overcurrent fault of load side (twice of the rated load current) is shown in Fig. 28. The SSCB in bus side is tripped when the current reaches the negative threshold. Thus, for the protection design of Super-UPS, the overcurrent threshold of load side should be less than twice of the rated load current.

V. Conclusion

In this paper, a fast protection scheme based on the fault-current direction is proposed for a Super-UPS, which is a compact and high-surety power-supply system. The scheme achieves fast fault detection and location based on the direction of current. The protection strategy coordinated with converters, which is based on the fault-current detection and dc-bus voltage detection, is investigated to achieve the uninterruptable load power. The rules of threshold setting are introduced for reliable operation of protection. Different thresholds for two directions are set to distinguish the module fault and busbar fault. The protection scheme does not rely on any communication, so a high-speed and a high-reliable protection is achieved. Besides, an improved fault-current measurement, which reduces the current-measurement error caused by the stray inductor of SSCB, is proposed to guarantee an accurate operation of protection for rapidly rising fault current. Finally, the proposed protection strategy and improved current measurement are verified on the platform of the Super-UPS. The proposed protection scheme can be applied in systems that have similar characteristics with Super-UPS, such as electric-vehicle charging stations with integrated photovoltaic and battery energy storage, dc UPS for IDC, etc. However, if the proposed scheme is applied to general dc microgrids and distribution line faults, other topologies and operation conditions should be considered, and further studies are needed.

Appendix

A. Threshold Setting for Modules in Super-UPS

Take the bidirectional dc/dc module in Super-UPS as an example, the parameters used for the threshold calculation is shown in Table VI.

TABLE VI
Parameters Used for Threshold Calculation

Item	Value	Item	Value
Negative Rated Current (I_{r_n})	-40 A	DC Bus Capacitor (C_{bus})	400 μF
Down-limit of Sampling Method (I_{sam_down})	120 A	$I_{90\%}$	-2.3 kA
The Maximum Transient Current (I_{dy})	-51 A	Maximum Protection delay (t_d)	2.7 μs
Maximum Current (I_{pd_max}) of IGBT in SSCB	1.3 kA	Maximum di/dt (k_{i_max})	30 A/μs
Maximum Current (I_{cap_max})of DC Capacitors	8 kA	Reliability Factor (K_{rel1}, K_{rel2})	1

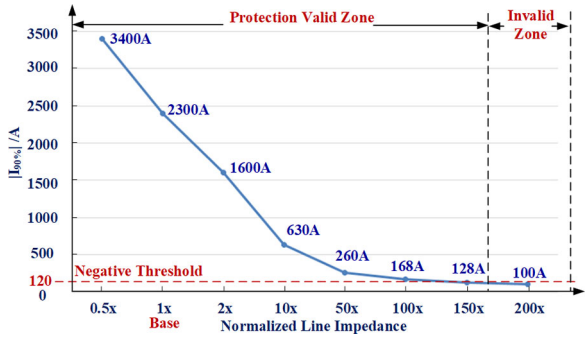

Fig. 29. Relationship between normalized line impedance and $I_{90\%}$.

According to (3), the threshold for negative direction is set to be 120 A. The threshold for the positive direction is 360 A. Besides, the down limit of bus voltage V_{down} for the source module is set to be 720 V. The up limit V_{up} is 780 V based on (5).

B. Influence of Line Impedance on Protection Scheme

According to (3), in order to avoid malfunctions of protection, the negative threshold should be less than $I_{90\%}$ which is the fault current value when the dc-bus voltage drops to 90% of the rated bus voltage. Based on simulations, Fig. 29 shows the relationship between the $I_{90\%}$ and normalized line impedance for CRC fault in Fig. 19. The values of line parameters given in Table V are regarded as the base values ("1x"). For example, "10x" means that each line parameter in Fig. 19 equals 10 times of the value given in Table V. It can be seen that $I_{90\%}$ is not large enough to trip the threshold only when the line impedance is larger than 200 times of the base value. However, in this situation, the maximum line inductance among modules reaches 1.76 mH, and the line distance is approximately 3.8 km, which is too long for the compact power supplies and UPS'. Thus, for compact power supplies, the fault current is large enough to trip the threshold when the short-circuit fault occurs.

References

[1] D. Xu, H. Li, Y. Zhu, K. Shi, and C. Hu, "High-surety microgrid: Super uninterruptable power supply with multiple renewable energy sources," *Electr. Power Compon. Syst.*, vol. 43, no. 8–10, pp. 839–853, Jun. 15, 2015.
[2] *IEEE Recommend Practice for 1 kV to 35 kV Medium-Voltage DC Power System on Ship*, IEEE Standard 1709, 2010.

[3] F. Liu, W. Liu, X. Zha, H. Yang, and K. Feng, "Solid-state circuit breaker snubber design for transient overvoltage suppression at bus fault interruption in low-voltage DC microgrid," *IEEE Trans. Power Electron.*, vol. 32, no. 4, pp. 3007–3021, Apr. 2017.
[4] C. Meyer and R. W. De Doncker, "Solid-State circuit breaker based on active thyristor topologies," *IEEE Trans. Power Electron.*, vol. 21, no. 2, pp. 450–458, Mar. 2006.
[5] R. Schmerda, R. Cuzner, R. Clark, D. Nowak, and S. Bunzel, "Shipboard solid-state protection: Overview and applications," *IEEE Electrific. Mag.*, vol. 1, no. 1, pp. 32–39, Sep. 2013.
[6] Z. J. Shen, G. Sabui, Z. Miao, and Z. Shuai, "Wide-bandgap solid-state circuit breakers for DC power systems: Device and circuit considerations," *IEEE Trans. Electron. Devices*, vol. 62, no. 2, pp. 294–300, Feb. 2015.
[7] Q. Huang, X. Zhou, and Z. Xu, "Solid-state DC circuit breaker," US Patent 2003/0183838, Oct. 2, 2003.
[8] R. M. Cuzner and G. Venkataramanan, "The status of DC micro-grid protection," in *Proc. IEEE Ind. Appl. Soc. Annu. Meet.*, Oct. 2008, pp. 1–8.
[9] L. Tang and B.-T. Ooi, "Locating and isolating DC faults in multi-terminal DC systems," *IEEE Trans. Power Del.*, vol. 22, no. 3, pp. 1877–1884, Jul. 2007.
[10] P. Cairoli and R. A. Dougal, "Fault detection and isolation in medium-voltage DC microgrids: Coordination between supply power converters and bus contactors," *IEEE Trans. Power Electron.*, vol. 33, no. 5, pp. 4535–4546, May 2018.
[11] M. Monadi, C. Gavriluta, A. Luna, J. I. Candela, and P. Rodriguez, "Centralized protection strategy for medium voltage DC microgrids," *IEEE Trans. Power Del.*, vol. 32, no. 1, pp. 430–440, Feb. 2017.
[12] M. Farhadi and O. A. Mohammed, "A new protection scheme for multi-bus DC power systems using an event classification approach," *IEEE Trans. Ind. Appl.*, vol. 52, no. 4, pp. 2834–2842, Jul.–Aug. 2016.
[13] J. D. Park, J. Candelaria, L. Ma, and K. Dunn, "DC ring-bus microgrid fault protection and identification of fault location," *IEEE Trans. Power Del.*, vol. 28, no. 4, pp. 2574–2584, Oct. 2013.
[14] E. Sortomme, S. S. Venkata, and J. Mitra, "Microgrid protection using communication-assisted digital relays," *IEEE Trans. Power Del.*, vol. 25, no. 4, pp. 2789–2796, Oct. 2010.
[15] A. Maqsood and K. Corzine, "DC microgrid protection: Using the coupled-inductor solid-state circuit breaker," *IEEE Electrific. Mag.*, vol. 4, no. 2, pp. 58–64, Jun. 2016.
[16] S. D. A. Fletcher, P. J. Norman, S. J. Galloway, and G. M. Burt, "Determination of protection system requirements for DC unmanned aerial vehicle electrical power networks for enhanced capability and survivability," *IET Elect. Syst. Transp.*, vol. 1, no. 4, pp. 137–147, Dec. 2011.
[17] A. A. S. Emhemed, K. Fong, S. Fletcher, and G. M. Burt, "Validation of fast and selective protection scheme for an LVDC distribution network," *IEEE Trans. Power Del.*, vol. 32, no. 3, pp. 1432–1440, Jun. 2017.
[18] M. E. Baran and N. R. Mahajan, "Overcurrent protection on voltage-source-converter-based multiterminal DC distribution systems," *IEEE Trans. Power Del.*, vol. 22, no. 1, pp. 406–412, Jan. 2007.
[19] M. Fang, L. Fu, R. Wang, and Z. Ye, "Coordination protection for DC distribution network in DC zonal shipboard power system," in *Proc. Int. Conf. Adv. Power Syst. Automat. Protection*, Oct. 2011, vol. 1, pp. 418–421.
[20] D. Salomonsson, L. Soder, and A. Sannino, "Protection of low-voltage DC microgrids," *IEEE Trans. Power Del.*, vol. 24, no. 3, pp. 1045–1053, Jul. 2009.
[21] E. Cinieri, A. Fumi, V. Salvatori, and C. Spalvieri, "A new high-speed digital relay protection of the 3-kVdc electric railway lines," *IEEE Trans. Power Del.*, vol. 22, no. 4, pp. 2262–2270, Oct. 2007.
[22] E. Christopher, M. Sumner, D. W. P. Thomas, X. Wang, and F. de Wildt, "Fault location in a zonal DC marine power system using active impedance estimation," *IEEE Trans. Ind. Appl.*, vol. 49, no. 2, pp. 860–865, Mar.–Apr. 2013.
[23] R. Mohanty and A. K. Pradhan, "Protection of smart DC microgrid with ring configuration using parameter estimation approach," *IEEE Trans. Smart Grid*, to be published, doi: 10.1109/TSG.2017.2708743.
[24] S. D. A. Fletcher, P. J. Norman, S. J. Galloway, P. Crolla, and G. M. Burt, "Optimizing the roles of unit and non-unit protection methods within DC microgrids," *IEEE Trans. Smart Grid*, vol. 3, no. 4, pp. 2079–2087, Dec. 2012.
[25] R. Li, L. Xu, and L. Yao, "DC fault detection and location in meshed multiterminal HVDC systems based on DC reactor voltage change rate," *IEEE Trans. Power Del.*, vol. 32, no. 3, pp. 1516–1526, Jun. 2017.
[26] S. Dhar, R. K. Patnaik, and P. K. Dash, "Fault detection and location of photovoltaic based DC microgrid using differential protection strategy," *IEEE Trans. Smart Grid*, vol. 9, no. 5, pp. 4303–4312, Sep. 2018.
[27] S. P. Gao, Q. Liu, and G. B. Song, "Current differential protection principle of HVDC transmission system," *IET Gener., Transmiss. Distrib.*, vol. 11, no. 5, pp. 1286–1292, Mar. 2017.
[28] S. D. A. Fletcher, P. J. Norman, K. Fong, S. J. Galloway, and G. M. Burt, "High-speed differential protection for smart DC distribution systems," *IEEE Trans. Smart Grid*, vol. 5, no. 5, pp. 2610–2617, Sep. 2014.
[29] R. M. Cuzner and V. Singh, "Future shipboard MVdc system protection requirements and solid-state protective device topological tradeoffs," *IEEE J. Emerg. Sel. Topics Power Electron.*, vol. 5, no. 1, pp. 244–259, Mar. 2017.
[30] National instruments, 2017, How to measure voltage, current, and power. [Online]. Available: http://www.ni.com/white-paper/8198/en/
[31] A. Hooshyar and M. Sanaye-Pasand, "Accurate measurement of fault currents contaminated with decaying DC offset and CT saturation," *IEEE Trans. Power Del.*, vol. 27, no. 2, pp. 773–783, Apr. 2012.
[32] X. Tian and R. Moussanet, "Current measurement using switch voltage drop in IGBT DC circuit breaker application," in *Proc. 5th Eur. Conf. Power Electron. Appl.*, Sep. 1993, vol. 2, pp. 332–336.
[33] C. Yuan, M. A. Haj-ahmed, and M. S. Illindala, "Protection strategies for medium-voltage direct-current microgrid at a remote area mine site," *IEEE Trans. Ind. Appl.*, vol. 51, no. 4, pp. 2846–2853, Jul.–Aug. 2015.
[34] K. Satpathi, N. Thukral, A. Ukil, and M. A. Zagrodnik, "Directional protection scheme for MVDC shipboard power system," in *Proc. 42nd Annu. Conf. IEEE Ind. Electron. Soc.*, Florence, Italy, Oct. 2016, pp. 3840–3847.
[35] D. Jovcic, M. Taherbaneh, J. P. Taisne, and S. Nguefeu, "Offshore DC grids as an interconnection of radial systems: Protection and control aspects," *IEEE Trans. Smart Grid*, vol. 6, no. 2, pp. 903–910, Mar. 2015.
[36] G. Wawrzola, "Challenges of DC data center power distribution protection," in *Proc. 13th Int. Conf. Develop. Power Syst. Protection*, Mar. 2016, pp. 1–6.
[37] J. Yang, J. E. Fletcher, and J. O'Reilly, "Short-circuit and ground fault analyses and location in VSC-Based DC network cables," *IEEE Trans. Ind. Electron.*, vol. 59, no. 10, pp. 3827–3837, Oct. 2012.
[38] H. Li, M. Chen, B. Yang, F. Blaabjerg, and D. Xu, "A fast fault protection based on direction of bus-side capacitor discharge current for a high-surety power supply," in *Proc. IEEE Energy Convers. Congr. Expo.*, Cincinnati, OH, USA, Oct. 2017, pp. 542–549.

Haijin Li (S'13) received the B.S. degree in electrical engineering in 2010, from Zhejiang University, Hangzhou, China, where he is currently working toward the Ph.D. degree.

He was supported by the China Scholarship Council to visit and work with the Department of Energy Technology, Aalborg University, Aalborg, Denmark, from 2016 to 2017. His current research interests include protection and controls of multiple energy storage systems and dc mircrogirds.

Min Chen (M'06) received the B.S. and Ph.D. degrees in power electronics from Zhejiang University, Hangzhou, China, in 1998 and 2004, respectively.

He is currently an Associate Professor of College of electrical engineering with Zhejiang University. His research interests include power quality control, high-frequency high-power conversion, and renewable energy power conversion systems.

Boping Yang received the B.S. degree in electrical engineering from Tianjin University, Tianjin, China, in 2013. He received the M.S. degree in power electronics from Zhejiang University, Hangzhou, China, in 2016.

His research interests include wireless power transfer and protection of power electronics systems. He is currently a Senior Engineer with Huawei Technologies Co., Ltd.

Frede Blaabjerg (S'86–M'88–SM'97–F'03) received the Ph.D. degree in electrical engineering from Aalborg University, Aalborg, Demark, in 1995.

He was with ABB-Scandia, Randers, Denmark, from 1987 to 1988. He became an Assistant Professor in 1992, an Associate Professor in 1996, and a Full Professor of power electronics and drives in 1998. In 2017, he became a Villum Investigator. He is Honoris Causa with the University Politehnica Timisoara, Timişoara, Romania, and Tallinn Technical University, Tallinn, Estonia. He has published more than 500 journal papers in the fields of power electronics and its applications. He is the co-author of two monographs and editor of 7 books in power electronics and its applications. He was the Editor-in-Chief for the IEEE TRANSACTIONS ON POWER ELECTRONICS from 2006 to 2012. He has been a Distinguished Lecturer for the IEEE Power Electronics Society from 2005 to 2007 and also for the IEEE Industry Applications Society from 2010 to 2011 as well as 2017 to 2018. His current research interests include power electronics and its applications such as in wind turbines, PV systems, reliability, harmonics and adjustable speed drives.

Dr. Blaabjerg is the recipient of 26 IEEE Prize Paper Awards, the IEEE PELS Distinguished Service Award in 2009, the EPE-PEMC Council Award in 2010, the IEEE William E. Newell Power Electronics Award 2014, and the Villum Kann Rasmussen Research Award 2014. In 2018 he was the President Elect of IEEE Power Electronics Society. He was nominated in 2014, 2015, 2016, and 2017 by Thomson Reuters to be among the Most 250 Cited Researchers in Engineering in the World.

Dehong Xu (M'94–SM'09–F'13) received the B.S., M.S., and Ph.D. degrees from Zhejiang University, Hangzhou, China, in 1983, 1986, and 1989, respectively.

He was a Visiting Scholar with the University of Tokyo, Japan, from June 1995 to May 1996. Since 1996, he has been a Full Professor with the College of Electrical Engineering, Zhejiang University, China. From June to December 2000, he was a Visiting Professor with Center for Power Electronics Systems, Virginia Tech, Blacksburg, VA, USA. From February to April 2006, he was a Visiting Professor with ETH Zurich, Zurich, Switzerland. His current research interests include power-electronics topology and control, power conversion for energy saving and renewable energy. He has authored or coauthored six books and more than 160 IEEE Journal or Conference papers. He owns more than 40 Chinese patents and 3 U.S. patents. He is an Associate Editor for the IEEE TRANSACTIONS ON POWER ELECTRONICS.

Dr. Xu is the recipient of four IEEE journal or conference paper awards. From 2013, he is the President of the China Power Supply Society. He is an At-Large Adcom Member of the IEEE Power Electronics Society from 2017 to 2019. He is the IEEE PELS Distinguish Lecturer in 2015–2017. In 2016, he received the IEEE PELS R. D. Middlebrook Achievement Award.